Variation of dendrite arm spacing in Al-rich Zn–Al off-eutectic alloys

N. TUNCA, R. W. SMITH
Department of Metallurgical Engineering, Queen's University, Kingston, Canada

Primary and secondary arm spacings were measured in various unidirectionally solidified Al-rich Zn–Al off-eutectic alloys. In order to determine the influence of convective processes on dendrite arm spacings, freezing was carried out both vertically upwards and downwards, and over a wide range of growth rates. The primary arm spacing parameter (d_1) has been correlated with the growth rate (R), the temperature gradient in the liquid immediately ahead of the solid/liquid interface (G_L) and the bulk alloy composition (C_0). Similar correlations were made for the secondary arm spacing (d_2). In addition, d_2 values were found to be related to the local solidification time (t_f). It was observed that the relationship $R^k G^m d_1 = K$, the primary arm spacing, and $R^{\ell} d_2 = K'$, secondary arm spacing, were obeyed (K and K' are constants). In addition, the effects of solute gradient-induced convection on the extent of macrosegregation in these alloys have been determined as a function of composition and growth rate.

1. Introduction

In metals and other systems, dendritic growth, the most common form of freezing, takes place with relatively small entropies of transformation. Dendritic or branched growth is based on the coupling of two seemingly independent growth processes: the steady-state propagation of the dendrite main stem and the non-steady-state evolution of dendrite branches. The non-steady-state nature of the side-branches controls their spacing and also the related, technically important scale of segregation. It has also been suggested that the branching mechanism itself might influence the steady-state growth of the dendrite main stem [1].

There have been several attempts in the recent past to develop a comprehensive theory of steady state unidirectional solidification [1–8]. In these studies, dendrite spacings have been correlated independently with growth rate and temperature gradient in the liquid, and also with the alloy composition. Moreover, tip radius of curvature, tip temperature, and tip concentration are predicted as functions of growth rate and temperature gradient. The characteristics of dendritic growth in organic systems and pure metals are relatively well understood, but the agreement between theory and experiment is not as complete for dendritic growth in metallic alloys under unidirectional solidification conditions [9–14], hence the present study.

The major morphological features of a dendrite interface are primary dendrite arm spacing, d_1, secondary dendrite arm spacing, d_2, and the dendrite tip radius, r_t. Once the primary arm spacing is established, it does not change during or after solidification. This is not the case, however, for the secondary arms, which undergo a "ripening" (coarsening) process [15–17]. For metal systems, ripening can be observed experimentally through examination of the microstructure after complete solidification or after a period of steady-state growth terminated by rapid quenching. d_1 can be measured very close to the quenched interface in a transverse cross section [11] and d_2 from a longitudinal cross section after complete solidification [4, 15].

During alloy solidification convective transport is usually present and influences growth kinetics, impurity incorporation, compositional homogeneity, morphological stability, and nucleation characteristics. Recently, there has been extensive research to establish the effects of fluid flow on solidification and on the properties of the resulting solid [18–22]. In the upward solidification of an alloy with a solute more dense than the solvent and a partition coefficient (k_0) less than unity, the macroscopic interface shape becomes curved due to the flow of liquid into local non-planar areas [14, 23]. The increased solute content further retards the growth in these regions, causing the interface to lag further behind. This is the result of what is termed gravitational or solutal convection [11, 14, 23]. In the downward solidification of similar alloys, an unstable density gradient parallel to the growth direction can also lead to solutal convection [22].

In the present work, experiments were carried-out to obtain further data on dendritic growth in order to better test current theories. Zn–Al off-eutectic alloys containing 6.5, 8.0 and 11.0% aluminium were solidified unidirectionally both upwards and downwards. The growth rate, R, was varied from 3 to 1000 $\mu m\,sec^{-1}$ and the liquid temperature gradient, G_L, from 28 to 120° C cm^{-1}. Primary and secondary dendrite arm spacings were measured and correlated with R and G_L. These results are compared with the predictions of current theories proposed for dendritic growth. Finally, the microstructure and macrosegregation observed during upward and downward solidification of these alloys are qualitatively described.

0022–2461/88 $03.00 + .12

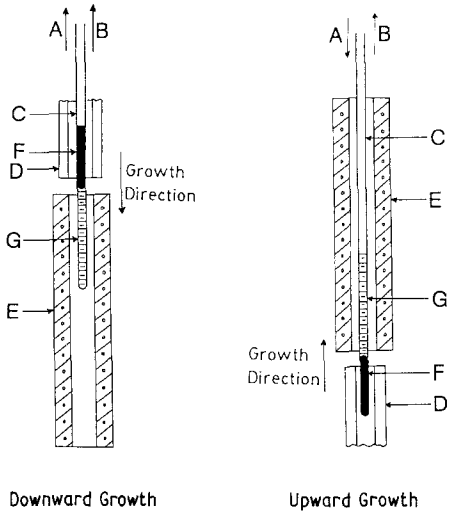

Figure 1 Schematic view of directional growth apparatus. (A) Direction of specimen tube movement. (B) Connection of drive unit. (C) Specimen tube. (D) Cooling device. (E) Tube furnace. (F) Solid. (G) Melt.

2. Experimental procedure

Zn–Al off-eutectic alloys (6.5, 8.0 and 11.0% aluminium) prepared from 99.99% zinc and 99.999% aluminium. The alloys were cast into 8 mm rods and then swaged to 4 mm diameter. The rods were sealed in graphite-coated quartz tubes, under a partial pressure of argon. Samples were unidirectionally solidified using the Bridgman-type furnace arrangement shown in Fig. 1, and quenched into a water bath at a certain stage of solidification in order to delineate the topography of the solid/liquid interface.

The temperature of the growing alloy was recorded using a 1.0 mm O.D. coaxial chromel–alumel thermocouple, and from the temperature against time trace, i.e. the cooling curve, the temperature gradient in the liquid at the growth front was measured. In the present series of experiments, the temperature gradient was varied from 28 to 120° C cm^{-1} (2.8×10^{-3} to 1.2×10^{-2} ° C μm^{-1}) and the growth rate from 3 to 1000 μm sec^{-1}.

Both transverse and longitudinal sections were cut from each specimen and mounted in cold-setting resin. These were polished and etched for a few seconds in a solution containing 5 g CrO_3, 0.5 g Na_2SO_4 and 100 ml H_2O followed by rinsing in a solution of 20 g CrO_3 and 100 ml H_2O before optical examination.

3. Results and discussion

3.1. Primary and secondary arm spacing

The variations in primary and secondary arm spacings, d_1 and d_2 respectively, with growth rate at constant temperature gradients are shown in Figs 2 and 3. It can be seen that both spacings decrease with increasing growth rate. The changes of d_1 and d_2 with R are essentially linear when $R > 10\,\mu$m sec^{-1} and G_L is kept approximately at 75 ± 6° C cm^{-1}; the same trend is also followed for G_L equal to 105 ± 9° C cm^{-1} or 120 ± 10° C cm^{-1}. The proportionality equations between primary arm spacing d_1, and growth rate for different compositions and temperature gradients, using a least-square linear regression analysis, are given in Table I; examination of these indicates that d_1 is proportional to R^{-k} for $R > 10\,\mu$m sec^{-1}. The proportionality equation calculated for the relationship between primary arm spacing and growth rate at

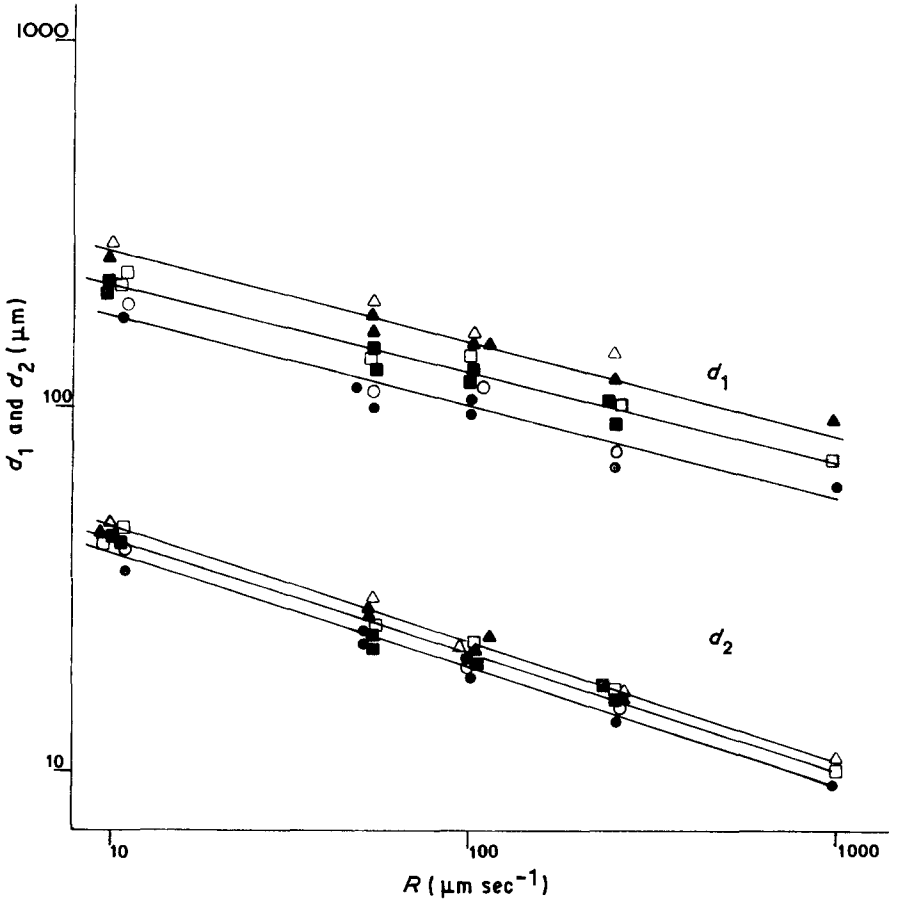

Figure 2 Variation of primary and secondary arm spacings (d_1 and d_2) with growth rate (R). $G_L = 75$° C cm^{-1}. (○) 6.5% Al–Zn, (□) 8.0% Al–Zn, (△) 11.0% Al–Zn. Open symbols: downward solidification, closed symbols: upward solidification.

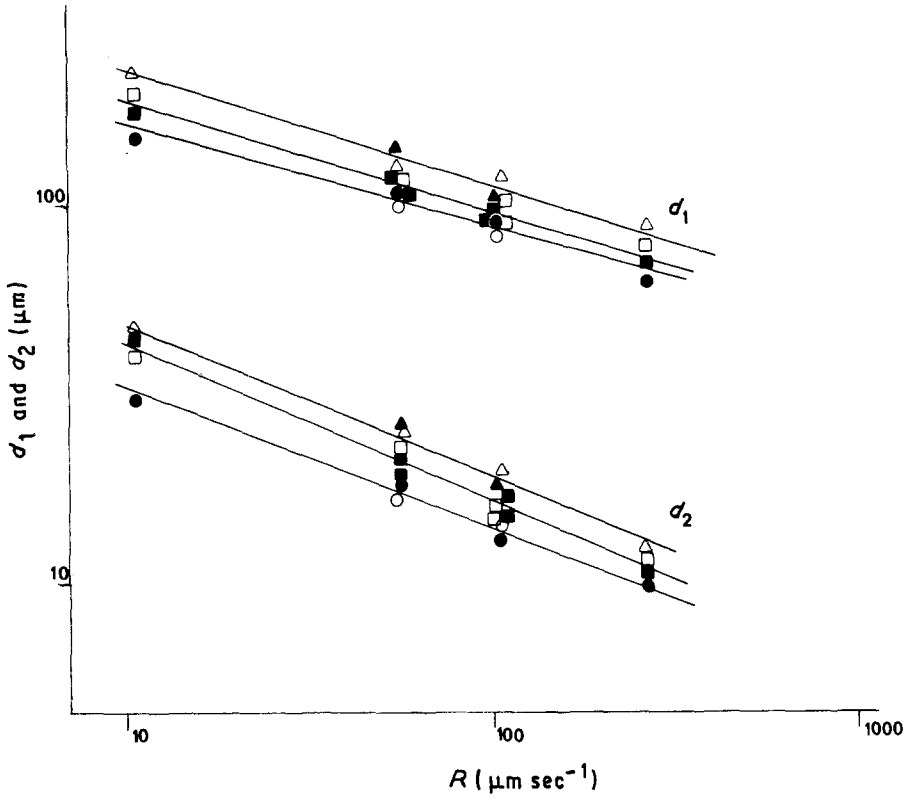

Figure 3 Variation of primary and secondary arm spacings (d_1 and d_2) with growth rate (R). G_L = 105° C cm^{-1} for 6.5% Al–Zn (○) and G_L = 120° C cm^{-1} for 8.0 (□) and 11.0% (△) Al–Zn. Open symbols: downward solidification, closed symbols: upward solidification.

G_L = 75° C cm^{-1}, $d_1 \alpha R^{-0.25 \pm 0.02}$, is in good agreement with that obtained by Kurz and Fisher [4, 25] and Hunt [29]. When the temperature gradients were increased to 105 or 120° C cm^{-1}, however, a deviation occurred from these theoretical predictions.

For $R > 10\,\mu m\,sec^{-1}$, d_2 was found to be proportional to $R^{-\ell}$ where ℓ is 0.33 ± 0.02 when G_L = 75° C cm^{-1}, ℓ = 0.38 ± 0.02 for G_L = 105° C cm^{-1} and 0.42 ± 0.02 for G_L = 120° C cm^{-1}. The value of the exponent when G_L = 75° C cm^{-1}, namely 0.33, is consistent with that obtained by Fleming [16, 17, 24] and Feuer [15] for the case of metal systems. Increasing R reduces the diffusion distance and, therefore, decreases both primary and secondary arm spacings. As shown in Figs 2 and 3, the slopes of the curves ($\partial d_1/\partial R$ and $\partial d_2/\partial R$) increase with increasing liquid temperature gradient, G_L. This implies that both the primary and secondary arm spacings decrease as G_L increases, thus confirming the dependency of spacing on G_L.

The effect of G_L on d_1 was investigated under conditions of constant composition and at two different growth velocities. The temperature gradient in the liquid was varied from 28 to 120° C cm^{-1}, and the results are shown in Fig. 4. The primary arm spacing decreases as G_L increases according to $d_1 \alpha G_L^{-m}$. The value of the exponent "m" depends on the velocity and equals 0.57 ± 0.04 at 53 μm sec^{-1} and 0.52 ± 0.04 at 100 μm sec^{-1}. Theoretical models proposed in the literature [4, 25, 29] to characterize primary arm spacing as a function of temperature gradient predict a $d_1 \alpha G_L^{-0.5}$ relationship. Experimental studies carried out in different systems [11, 26], either metallic or organic, showed a slight variation of the exponent "m" from the theoretical calculations, as also observed in our study. This is believed to be due to the dependency of "m" on the particular alloy system and the alloy composition used.

3.1.1. Tip radius

During medium and high growth rates, the tip radius of the dendrites (r_t) growing under conditions of unidirectional solidification can be expressed as [4, 25]

$$r_t = 2\pi \left(\frac{D\Gamma}{Rk_0\Delta T_0} \right)^{1/2} \quad (1)$$

where D is the diffusion coefficient of solute in the melt, Γ is the Gibbs-Thompson coefficient, R is the growth rate, k_0 is the distribution coefficient, and ΔT_0: freezing interval at C_0. Whilst r_t may not be determined directly in opaque systems, it may be calculated as a function of growth rate, using Equation 1. This has been done and the results are presented in Fig. 5.

TABLE I The proportionality equations between primary (d_1), or secondary (d_2) arm spacing and growth rate (R) for different bulk alloy compositions (C_0) and liquid temperature gradient ahead of the solid/liquid interface (G_L).

C_0 (wt % Al)	G_L (° C μm^{-1})	d_1 (μm)	d_2 (μm)
6.5% Al–Zn	0.0075	$d_1 = 321R^{-0.25 \pm 0.02}$	$d_2 = 86R^{-0.32 \pm 0.02}$
8.0% Al–Zn	0.0075	$d_1 = 373R^{-0.24 \pm 0.01}$	$d_2 = 92R^{-0.32 \pm 0.02}$
11.0% Al–Zn	0.0075	$d_1 = 475R^{-0.25 \pm 0.02}$	$d_2 = 102R^{-0.33 \pm 0.02}$
6.5% Al–Zn	0.0105	$d_1 = 319R^{-0.27 \pm 0.03}$	$d_2 = 79R^{-0.38 \pm 0.02}$
8.0% Al–Zn	0.0120	$d_1 = 378R^{-0.29 \pm 0.01}$	$d_2 = 114R^{-0.42 \pm 0.02}$
11.0% Al–Zn	0.0120	$d_1 = 469R^{-0.30 \pm 0.02}$	$d_2 = 124R^{-0.41 \pm 0.02}$

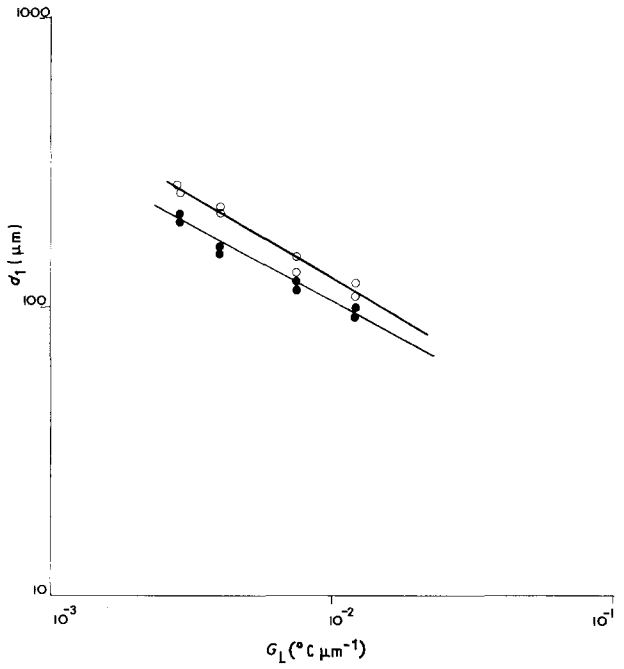

Figure 4 Effect of temperature gradient (G_L) on primary arm spacing (d_1) at two growth rates for 8.0% Al–Zn with downward solidification (○) $R = 53\,\mu m\,sec^{-1}$, (●) $R = 100\,\mu m\,sec^{-1}$.

This shows that tip radius decreases with increasing growth rate according to the $r_t R^{1/2} = K''$ relationship.

3.1.2. Peclet Numbers

Two of the important parameters in the analysis of diffusion-controlled dendritic growth, the solutal Peclet number (P_s) and thermal Peclet number (P_t), may be calculated from the relationships

$$P_s = \frac{r_t R}{2D} \tag{2}$$

and

$$P_t = \frac{r_t R}{2K_T} \tag{3}$$

where K_T is thermal diffusivity. Calculated solutal and thermal Peclet numbers are given in Fig. 6. Hence, whilst the solutal Peclet number varies from 0.0055 to 0.56, the thermal Peclet number increases from 1.3×10^{-6} to 14×10^{-6}. Both Peclet numbers decrease with decreasing growth rate. The diffusion length L, which is $2D/R$ or $2K_T/R$, decreases with increasing Peclet number. As a result, an increasing R reduces the diffusion distance (while P_s and P_t increase) and therefore decreases the d_1 spacing as shown in Figs 2 and 3. It is noted that the same values for D and K_T were used for each alloy since no other data were available. The fact that straight, near parallel lines are obtained suggests that this is reasonable assumption.

TABLE II The proportionality equation between secondary arm spacing (d_2) and local solidification time (t_f) for different bulk alloy compositions (C_0) and liquid temperature gradient ahead of the solid/liquid interface (G_L).

C_0 (wt % Al)	G_L (°C μm^{-1})	d_2 (μm) against t_f (sec)
6.5% Al–Zn	0.0075	$d_2 = 9.08 t_f^{0.32 \pm 0.02}$
8.0% Al–Zn	0.0075	$d_2 = 7.89 t_f^{0.32 \pm 0.02}$
11.0% Al–Zn	0.0075	$d_2 = 6.49 t_f^{0.33 \pm 0.02}$
6.5% Al–Zn	0.0105	$d_2 = 6.43 t_f^{0.38 \pm 0.02}$
8.0% Al–Zn	0.0120	$d_2 = 5.15 t_f^{0.42 \pm 0.02}$
11.0% Al–Zn	0.0120	$d_2 = 4.72 t_f^{0.41 \pm 0.02}$

3.1.3. Secondary dendrite arm coarsening

During steady-state dendritic growth, secondary arms begin to form very close to the tip of the dendrite main stem. It is known that they appear initially as a sinusoidal perturbation of a paraboloid. In this regime, the relationship between d_2 and r_t (tip radius) is independent of temperature gradient according to the "Scaling Law" [5, 8, 26, 27]. However, during coarsening of the secondary arms, the local solidification time (which is inversely proportional to G_L since $t_f = \Delta T_0 / G_L R$ where ΔT_0 = freezing interval at C_0) plays an important role [4, 15, 16, 17]. As a result, the secondary arm spacing decreases with increasing G_L.

The coarsening process is visualized to be analogous to the Ostwald ripening of precipitates in solids i.e. the smaller (larger curvature) secondary arms should disappear and feed the growth of the already larger arms due to surface energy considerations. As with the ripening of precipitates, the time dependence of d_2 is frequently correlated with t_f according to a power law

$$d_2 = A t_f^n \tag{4}$$

where A is constant for the alloy system used. Existing theoretical analyses suggest that the exponent has the value 0.33 [4, 15].

The local solidification time was measured in

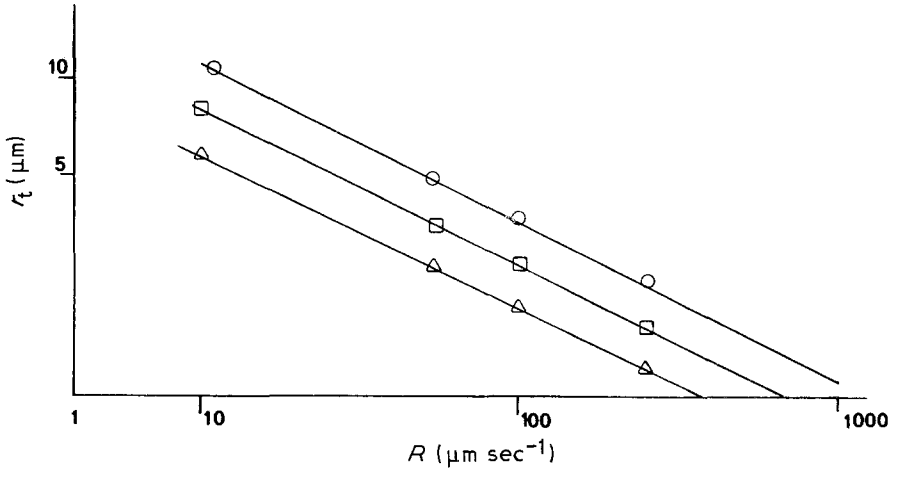

Figure 5 Dendrite tip radius (r_t) as a function of growth rate (R). (○) 6.5% Al–Zn, (□) 8.0% Al–Zn, (△) 11.0% Al–Zn.

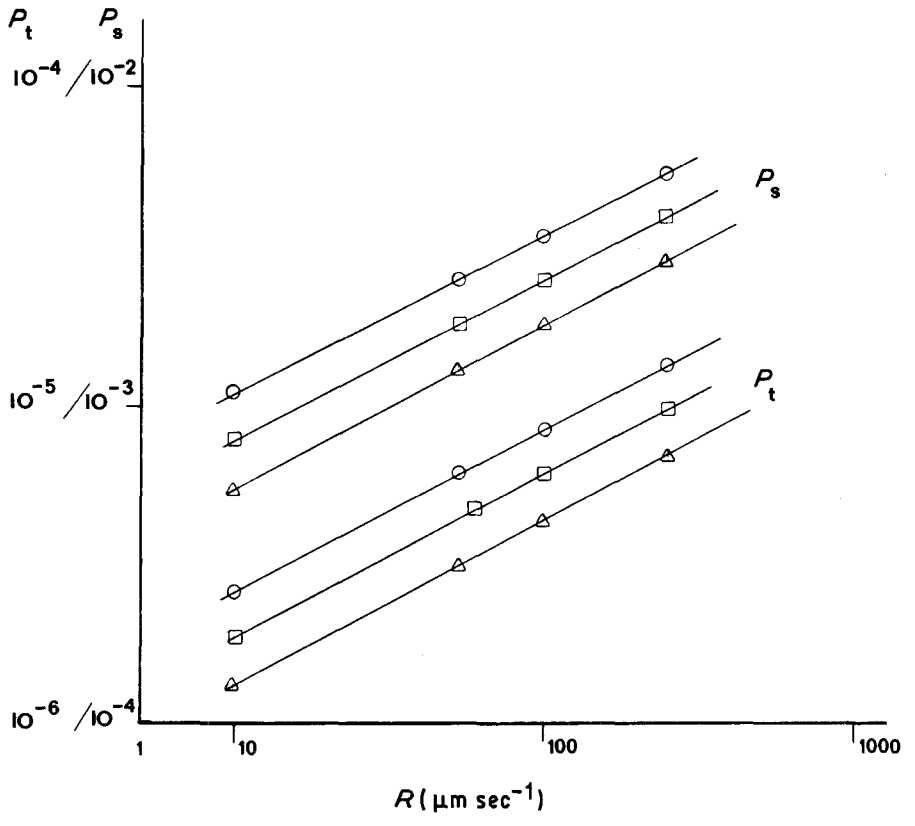

Figure 6 Variation of thermal (P_t) and solutal (P_s) Peclet numbers with growth rate (R). G_L = 75° C cm^{-1}. (○) 6.5% Al–Zn, (□) 8.0% AL–Zn, (△) 11.0% Al–Zn.

interrupted solidification experiments using the relationship

$$t_f = L/R \quad (5)$$

where L is the distance between the eutectic front (eutectic interface) and the plane of dendrite tips in quenched region.

As shown in Fig. 7 and Table II, the experimental relationship d_2 as a function of t_L at G_L = 75° C cm^{-1} is in good agreement with the theoretical calculations of Equation 3, i.e. $d_2 \alpha t_f^{0.33}$ ($d_2 \alpha R^{-0.33}$). However, the variation of d_2 in the $R > 10\,\mu m\,sec^{-1}$ regime was found to be proportional to $t_f^{0.38}$ or $t_f^{0.42}$ and $t_f^{0.41}$ instead of $t_f^{0.33}$ when G_L was increased to 105° C cm^{-1} or 120° C cm^{-1} respectively (Fig. 8 and Table II).

In addition to the effect of increased solidification time in increasing the dendrite arm spacing, it was found that for the same local solidification time that the dendrite arm spacing decreased with increased solute (wt % Al) content as shown in Figs 7 and 8. Many authors [13, 17, 30] have also reported that in metal systems, the rate of dendrite arm coarsening falls as the solute content is increased. Furthermore, the composition of the alloy affects the dendrite spacings d_1 and d_2. For example, the values of d_1 and d_2 increase as the Al concentration in the alloy

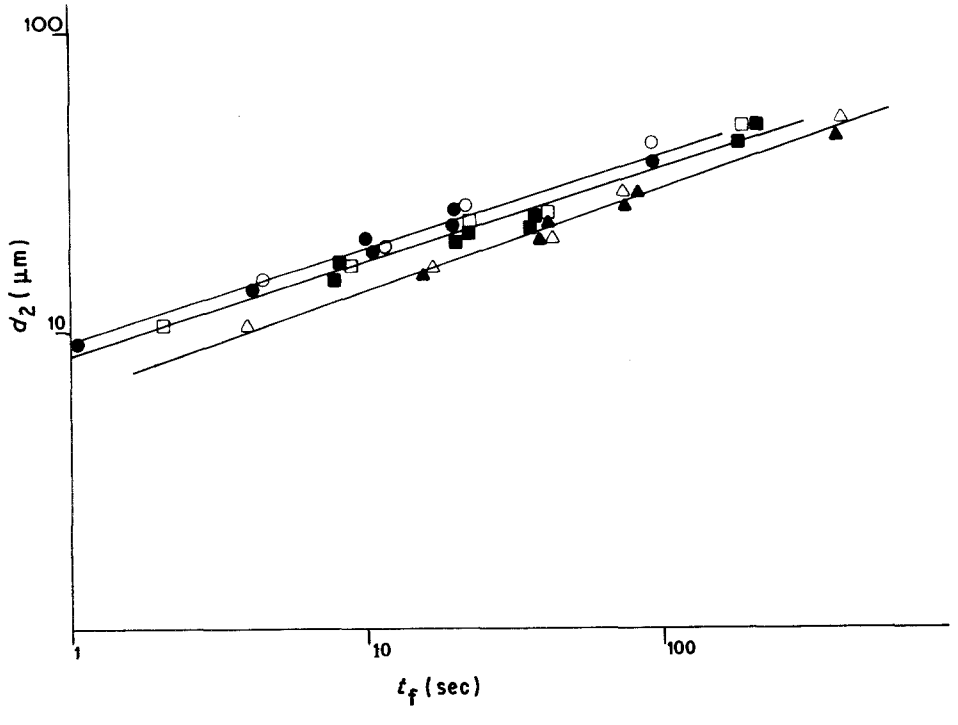

Figure 7 Variation of secondary arm spacing (d_2) with local solidification time (t_f). G_L = 75° C cm^{-1}. (○) 6.5% Al–Zn, (□) 8.0% Al–Zn, (△) 11.0% Al–Zn. Open symbols: downward solidification, closed symbols: upward solidification.

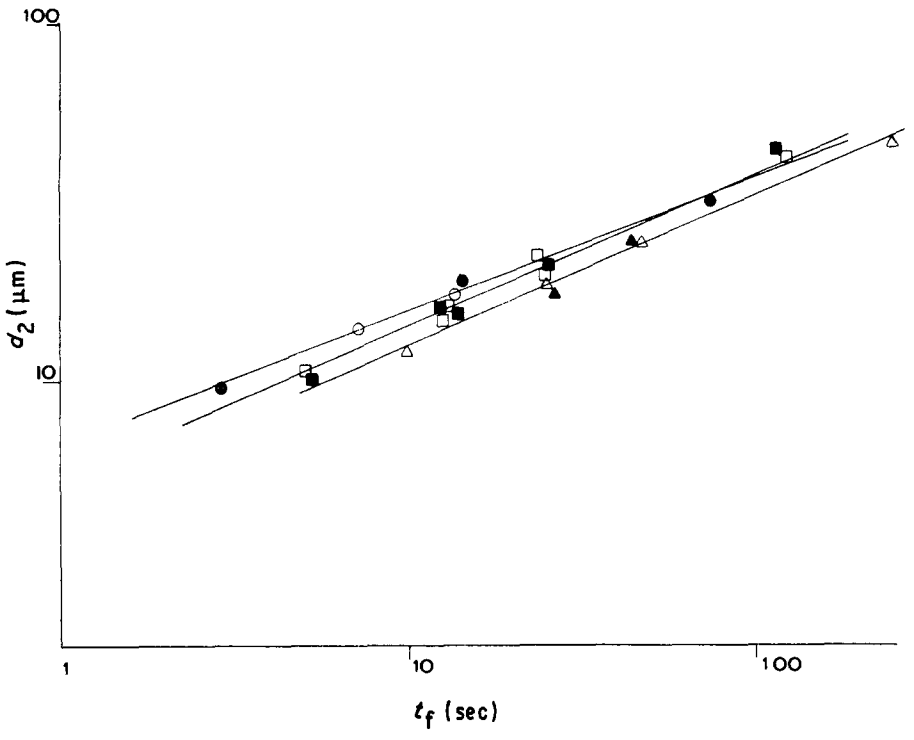

Figure 8 Variation of secondary arm spacing (d_2) with local solidification time (t_f). G_L = 105 and 120° C cm^{-1}. (○) 6.5% Al–Zn, (□) 8.0% Al–Zn, (△) 11.0% Al–Zn. Open symbols: downward solidification, closed symbols: upward solidification.

is increased for constant G_L and R values (Figs 2 and 3).

3.2. Microscopic observations

In the Al-rich off-eutectic alloys, one of the eutectic phases, β undergoes a eutectoid transformation upon cooling to 275° C, forming α (Al-rich) and η (Zn-rich) phases (Fig. 9). Fig. 10a shows the β-phase (AlZn, dendritic form) in (β + η) eutectic. A higher magnification micrograph of the β-phase (Fig. 10b) shows the actual eutectoid structure (α + η).

3.3. Effect of microsegregation

Convection induced by solute density variations will be inherently present in many off-eutectic melts. Its extent will depend on the composition versus density dependence and the growth direction.

3.3.1. Upward solidification

It is sometimes assumed that one method of eliminating gravitational convection in the melt is to maintain a negative vertical density gradient in the liquid. This may be achieved by solidifying the alloy vertically upwards in a system in which the solute being rejected at the interface is more dense than the bulk liquid. However, it is obvious that this may not be a remedy in this case. Zinc and aluminium have very different liquid densities, respectively 6.96 g ml^{-1} and 2.37 g ml^{-1}. During solidification of Al-rich Zn–Al off-eutectic alloys, the Zn-rich solute rejected at the Al-rich dendrite/liquid interface is denser than the surrounding liquid. At small growth rates (R < 10 μm sec^{-1}), any radial temperature gradient is expected to be more critical than at higher growth rates since this will promote the development of a

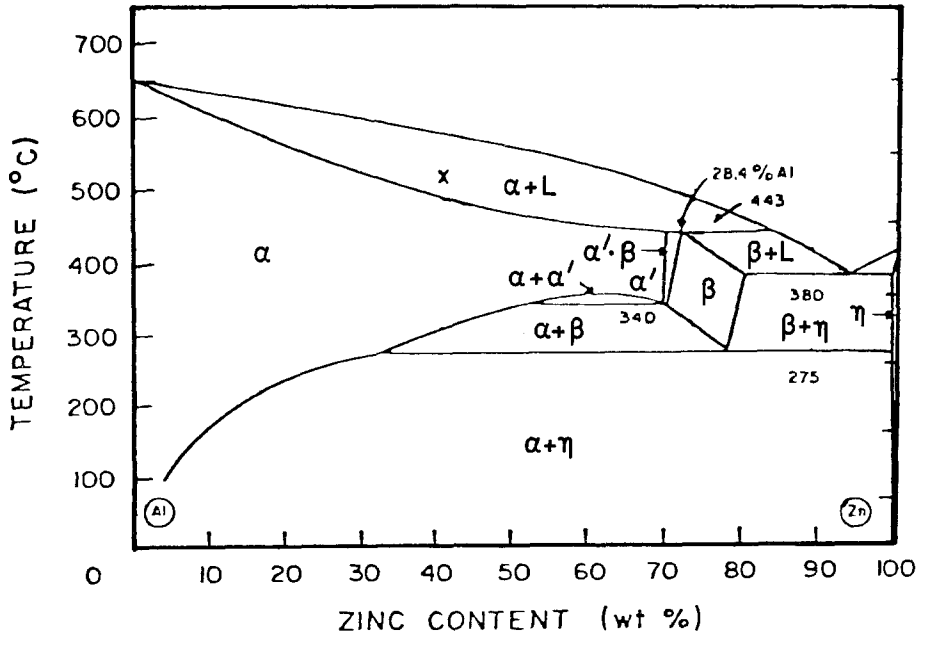

Figure 9 The binary Zn–Al equilibrium diagram.

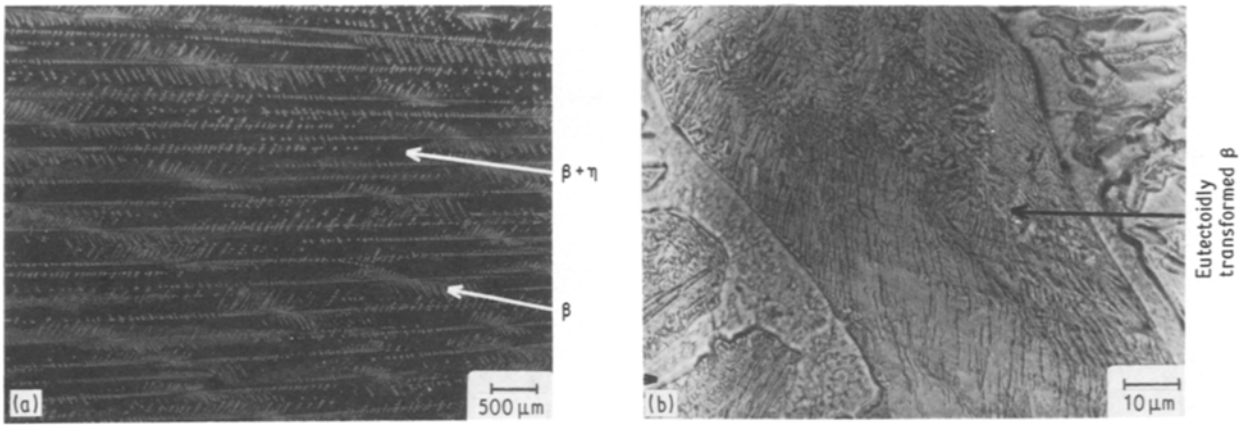

Figure 10 Microstructure of 6.5% aluminium Zn–Al off-eutectic alloy. (a) β (AlZn) dendrites in the $\beta + \eta$ eutectic mixture (b) Higher magnification of β phase: α (Al-rich) and η (Zn-rich eutectoid phase).

non-planar growth front. If the interface is planar, no fluid flow occurs. However, if the macroscopic interface lags slightly at one point then the more dense liquid, i.e. that liquid most rich in zinc, will flow into the retarded region forcing it to drop still further behind the overall interface. In the present series of experiments, a curved interface shape was observed at growth rates less than $10\,\mu m\,sec^{-1}$ during upward growth. Typical interface morphologies obtained from quenched samples are shown in Fig. 11a, b and c. Similar interface morphologies have been noted by Burden-Hebditch-Hunt [23] and Miyata-Suzuki-Uno [14] in Al-rich Al–Cu off-eutectic alloys and by the present authors in 6.5, 8.0 and 11.0% Al–Zn off-eutectic alloys grown vertically upward. The extent of macrosegregation was indicated by the change in volume fraction of dendrites along the length of the sample. In the range $10 < R < 1000\,\mu m\,sec^{-1}$ only a relatively small amount of macrosegregation is observed, i.e., the volume fraction of Al-rich dendrites was observed to have increased only slightly at the end of unidirectionally grown samples. This change can be accounted for by solutal diffusion processes (Fig. 6). When the growth rate is reduced still further, however, the dendrite front becomes increasingly irregular (Fig. 11b) because of the presence of enhanced solutal convection. Since regions of the interface may not display any pro-eutectic dendrites (Fig. 11c). This is shown in more detail in Fig. 12 ($R = 3\,\mu m\,sec^{-1}$). The microstructure changes from dendritic to lamellar eutectic growth across the sample.

3.3.2. Downward solidification

In contrast to the behaviour seen in upward solidification, the eutectic and dendritic interfaces in downward solidification are always nearly planar regardless of the growth rate (Fig. 13). There exists also a small degree of macrosegregation, observed at growth rates greater than $8\,\mu m\,sec^{-1}$, confirming the presence of slight solutal and thermal diffusion. The volume fraction of the Al-rich dendrites in the structure gradually decreased as solidification progressed at a growth rate of $8\,\mu m\,sec^{-1}$, as a result of the solutal convection. However, the structure still remained dendritic. Presumably, vigorous solutal convection should cause severe macrosegregation along the vertical direction at $R = 3\,\mu m\,sec^{-1}$. The solute being rejected is expected to be transported continuously into the bulk liquid far from the solid/liquid interface. As a result, the nominal bulk composition of the liquid gradually changes and becomes more Zn-rich, therefore the amount of Al-rich dendrites in the structure decreases accordingly. When the bulk liquid attains the eutectic composition, only eutectic growth is observed ($\beta + \eta$). Fig. 14 shows the variation of the structure of 11% Al–Zn alloy at growth rate of $3\,\mu m\,sec^{-1}$. Varying sample lengths did not change the content of the fully eutectic phase at the end of the samples (Table III).

In contrast to the downward solidification of the Al-rich Zn–Al off-eutectic alloys, a fairly homogeneous dendritic structure was observed throughout the samples of Zn-rich Zn–Al off-eutectic alloys in downward solidification, even at low growth rates ($R = 3\,\mu m\,sec^{-1}$). When the solidification direction was reversed (upward solidification), a similar structure was observed in these alloys as in the Al-rich Zn–Al off-eutectic alloys solidified downward. The percentage of the microstructure occupied by eutectic

TABLE III Concentration of the fully eutectic phase of Al-rich Zn–Al off-eutectic alloys solidified downward, $R = 3\,\mu m\,sec^{-1}$.

Alloy (wt % Al)	G_L (°C cm^{-1})	Length of grown sample (mm)	Length of fully eutectic structure (mm)	% of fully eutectic structure
6.5% Al–Zn	75	160	42	26.3
8.0% Al–Zn	75	69	18	26.1
8.0% Al–Zn	120	122	33	27.1
11.0% Al–Zn	75	66	17	25.8
11.0% Al–Zn	120	89	24	27.0
4.0% Al–Zn*	75	80	12	15

*Concentration of fully eutectic phase of Zn-rich Zn–Al off-eutectic alloy solidified upward, $R = 3\,\mu m\,sec^{-1}$.

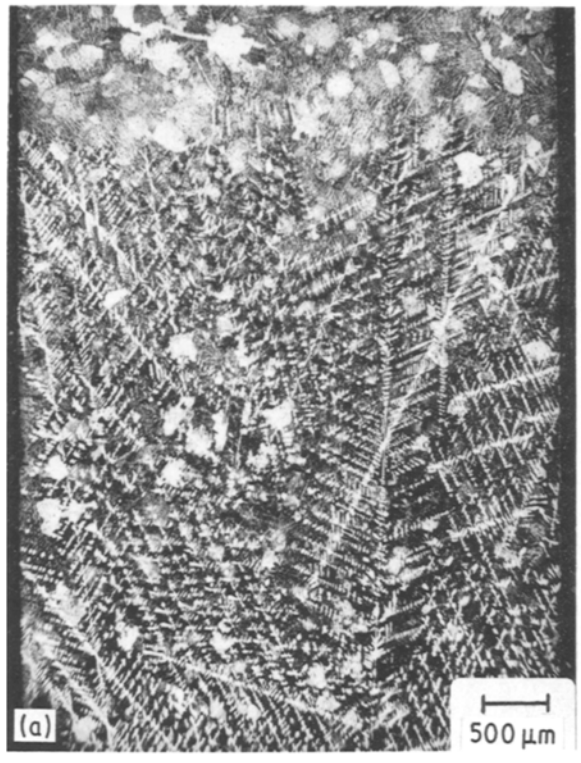

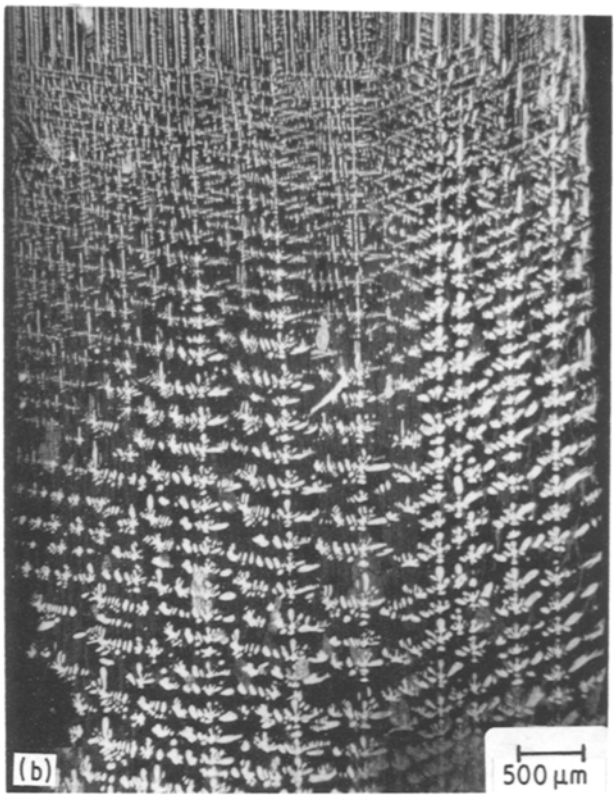

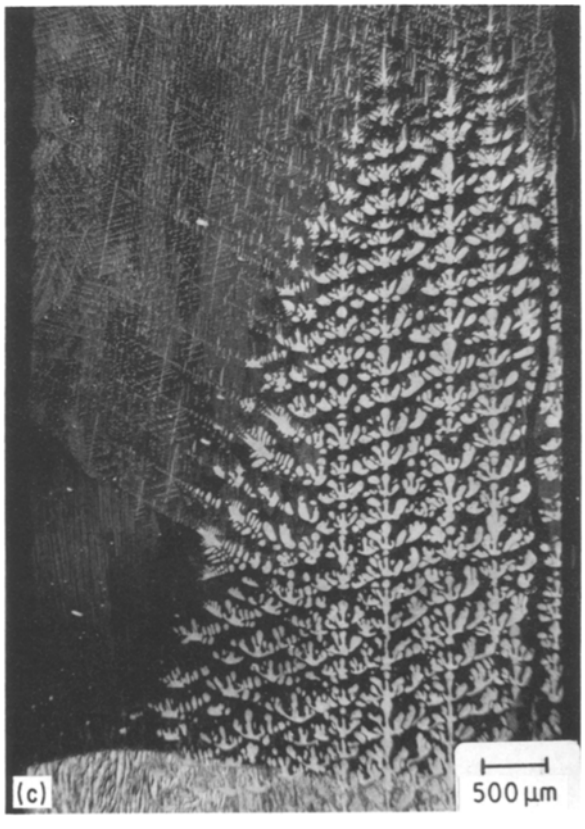

Figure 11 Longitudinal (or parallel) section of quenched interfaces of 8% Al–Zn alloy solidified upward. (5 mm diameter). $G_L = 75°C\,cm^{-1}$. (a) $R = 53\,\mu m\,sec^{-1}$, (b) $R = 8\,\mu m\,sec^{-1}$, (c) $R = 3\,\mu m\,sec^{-1}$.

of 4% Al–Zn alloy which is observed at the end of the sample is also given in Table III.

Thermal Rayleigh numbers, R_t, were calculated using the parameters given in Table IV. These are found to be 41 and 66 for $G_L = 75°C\,cm^{-1}$ and $G_L = 120°C\,cm^{-1}$ respectively. The calculated critical Rayleigh number for closed containers above which thermal convection is effective, has been given as 68 [28]. Thus the value $R_t = 66$ is very close to the critical value for the 5 mm tube diameter used in the present experiments. Now an increase in temperature gradient or the diameter of the tube increases the value of R_t. Thus in this case, it is expected that the thermal convection should contribute to the macrosegregation in addition to the contribution of solutal convection.

A model developed to calculate macrosegregation in dendritic growth of off-eutectic alloys will be presented in another paper in the near future. This model relates the growth rate, temperature gradient, composition and material properties to predict the convection patterns and subsequent macrosegregation as a function of the gravitational field present.

4. Conclusions

Al-rich Zn–Al off-eutectic alloys containing 6.5, 8.0 and 11.0% aluminium were solidified unidirectionally upward and downward and their morphological features were investigated as a function of growth rate and temperature gradient. Primary and secondary arm spacings were measured and used to determine whether equations of the form $d_1 R^k G^m = K$ for

TABLE IV Parameters used in calculations

D	Diffusion coefficient of solute in the melt	$5 \times 10^{-5}\,cm^2\,sec^{-1}$
Γ	Gibbs-Thomson coefficient	$40 \times 10^{-7}\,°C\,cm$
K_T	Thermal diffusivity [18]	$0.21\,cm^2\,sec^{-1}$
ν	Kinematic viscosity [18]	$3 \times 10^{-3}\,cm^2\,sec^{-1}$
g	Gravitational acceleration	$980\,cm\,sec^{-2}$
r	Radius of the tube	0.25 cm
α	Thermal expansion coefficient	$9 \times 10^{-5}\,(°C)^{-1}$
R_t	Thermal Rayleigh Number	$R_t = -\frac{g\alpha G_L r^4}{\nu K}$

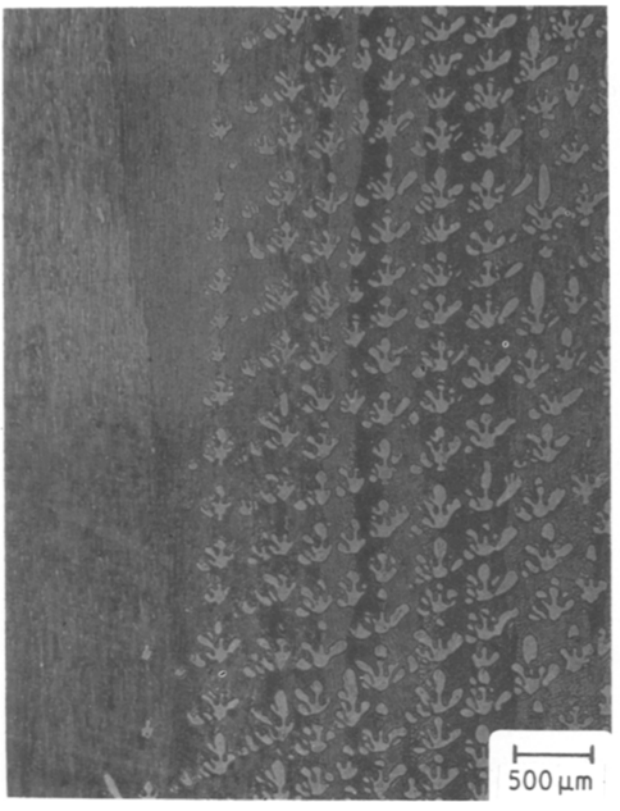

Figure 12 Dendritic structure of 6.5% Al–Zn alloy solidified upward at $R = 3\,\mu m\,sec^{-1}$. $G_L = 75°C\,cm^{-1}$. Note the structure change from dendritic to eutectic in transverse direction.

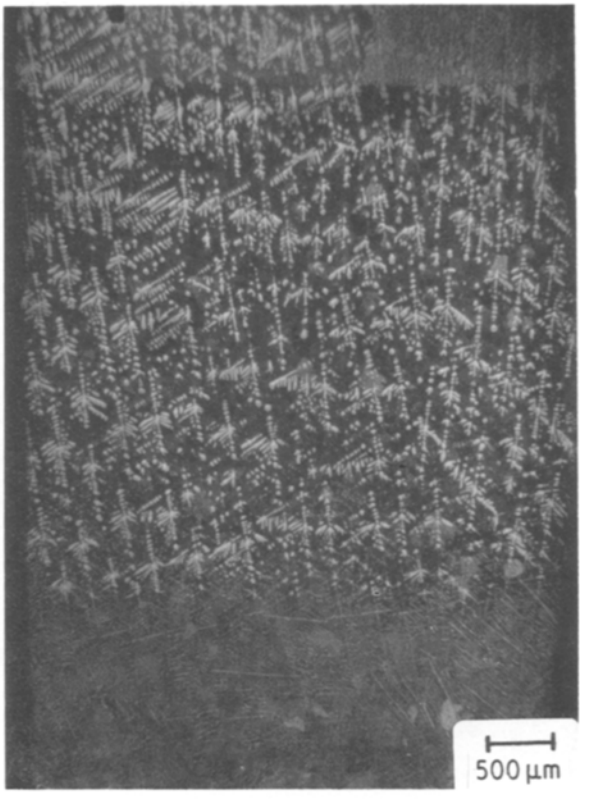

Figure 13 Longitudinal section of quenched interfaces of 8% Al–Zn alloy solidified downward at $R = 8\,\mu m\,sec^{-1}$.

primary arm spacing and $d_2R^{\ell} = K'$ for secondary arm spacing could be applied. The principal results can be summarized as follows

(i) Primary and secondary arm spacings vary with the growth rate. When $G_L = 75°C\,cm^{-1}$, observed growth rate exponents k and ℓ for d_1 and d_2 are found to be 0.25 ± 0.02 (or 0.24 ± 0.01) and 0.33 ± 0.02 (or 0.32 ± 0.02), which are in good agreement with those reported in previous works. They deviated slightly, however, for $G_L = 105$ and $120°C\,cm^{-1}$.

(ii) The primary arm spacing, d_1, decreases as temperature gradient in the liquid, G_L, increases. The value of the temperature gradient exponent m depends on the growth velocity and is equal to 0.57 ± 0.04 at $53\,\mu m\,sec^{-1}$ and 0.52 ± 0.04 at $100\,\mu m\,sec^{-1}$, both of which depart slightly from theoretical predictions.

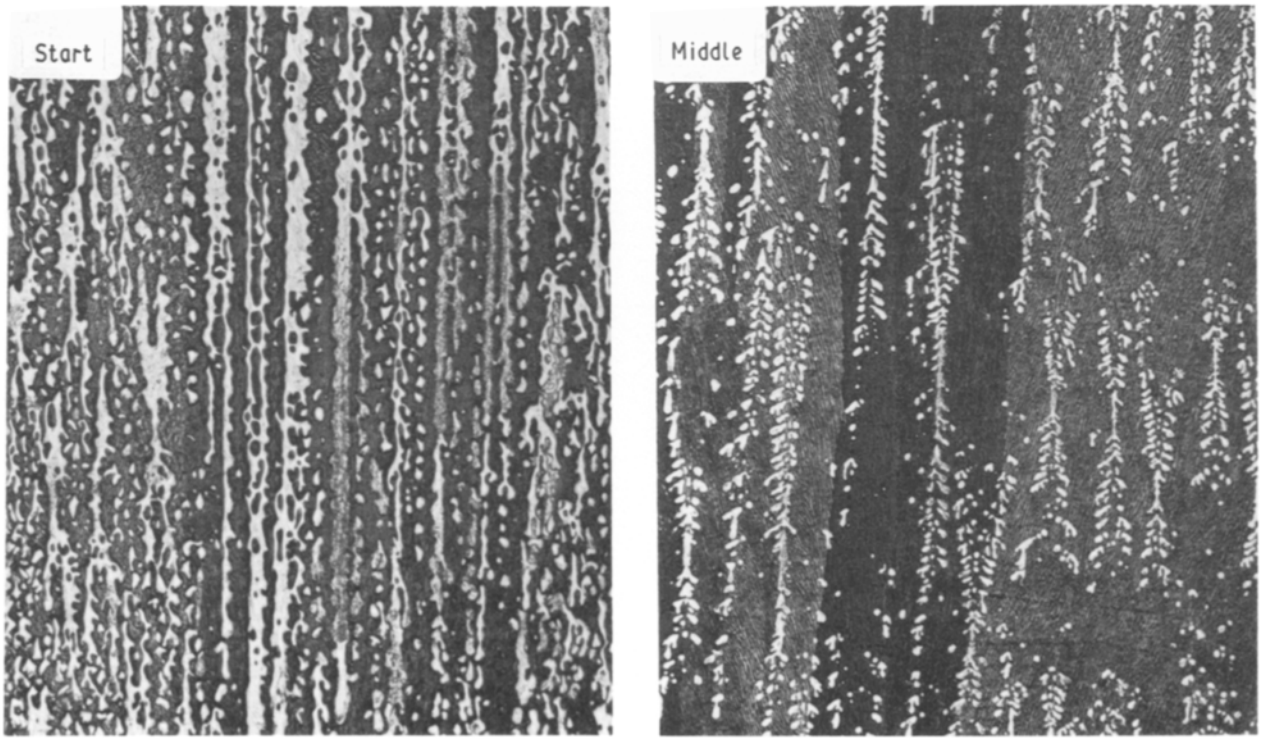

Figure 14 Variation of the structure of the 11% Al–Zn alloy solidified downward. $R = 3\,\mu m\,sec$. $G_L = 75°C\,cm^{-1}$.

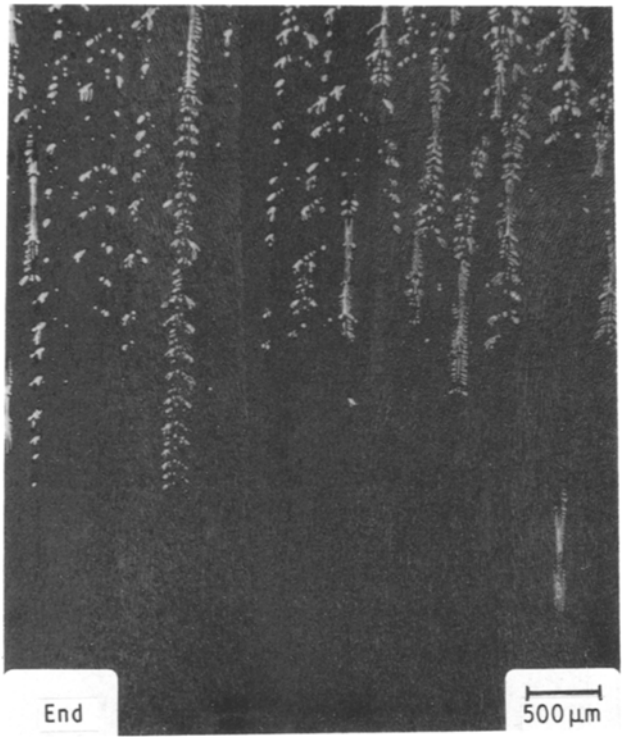

Figure 14 Continued.

(iii) The observed local solidification time versus d_2 relationship is consistent with theoretical calculations which give $d_2 = Kt_f^{0.33}$ (or $t_f^{0.32}$) for $G_L = 75°C\,cm^{-1}$, but it deviates slightly for $G_L = 105$ and $120°C\,cm^{-1}$.

(iv) Both upward and downward solidification conditions ensure a homogeneous melt composition without macrosegregation for $R > 10\,\mu m\,sec^{-1}$.

(v) Solute gradient-induced convection can cause extensive macrosegregation in Al-rich Zn–Al off-eutectic alloys when $R < 10\,\mu m\,sec^{-1}$. Vertical macrosegregation in downward and horizontal macrosegregation in upward growth for $R < 10\,\mu m\,sec^{-1}$ were more extensive than expected in these alloys. If the solid/liquid interface is kept planar, macrosegregation caused by solutal convection in conventional solidification (upward growth) could be avoided and so give homogeneous microstructures throughout the material for growth rates less than $10\,\mu m\,sec^{-1}$ as well as in faster growth rates.

Acknowledgements

The authors wish to thank Dr. M. Savas and L. Clapham for suggestions and revision of the manuscripts and to R. Lobb for technical assistance.

Appendix

Nomenclature:

d_1	Primary arm spacing, μm.
d_2	Secondary arm spacing, μm.
R	Growth rate, $\mu m\,sec^{-1}$.
G_L	Temperature gradient ahead of the solid/liquid interface, $°C\,\mu m^{-1}$ or $°C\,cm^{-1}$.
C_0	Bulk alloy composition, wt %.
K, K', K''	Constants.
k, m, ℓ, n	Exponents.
t_f	Local solidification time, sec.
ΔT_0	Freezing interval at C_0, °C.
L	Distance between eutectic front and the plane of dendrite tips, μm.
r_t	Tip radius of dendrites, μm.
D	Diffusion coefficient of solute in the melt, $cm^2\,sec^{-1}$ or $\mu m^2\,sec^{-1}$.
Γ	Gibb-Thomson coefficient, °C. cm or °C μm.
k_0	Distribution or partition coefficient.
K_T	Thermal diffusivity.
P_s	Solutal Peclet number.
P_t	Thermal Peclet number.
R_t	Thermal Rayleigh number.

References

1. S.-C. HUANG and M. E. GLICKSMAN, *Acta Metall.* **29** (1981) 701.
2. M. H. BURDEN and J. D. HUNT, *J. Cryst. Growth* **22** (1974) 109.
3. R. TRIVEDI, *ibid.* **49** (1980) 219.
4. W. KURZ and D. FISHER, "Fundamentals of Solidification" (Trans. Tech. Publications, Switzerland, 1984) p. 65.
5. I. JIN and G. R. PURDY, *J. Cryst. Growth* **23** (1974) 29.
6. V. LAXMANAN, *Acta Metall.* **33** (1985) 1023.
7. R. TRIVEDI and K. SOMBOONSUK, *ibid.* **33** (1985) 1051.
8. *Idem*, *ibid.* **33** (1985) 1061.
9. R. M. SHARP and A. HELLAWELL, *J. Cryst. Growth* **11** (1971) 77.
10. C. M. KLAREN, J. D. VERHOEVEN and R. TRIVEDI, *Metall. Trans. A*, **11A** (1980) 1853.
11. D. G. MCCARTNEY and J. D. HUNT, *Acta Metall.* **29** (1981) 1851.
12. T. OKAMOTO and K. KISHITAKE, *J. Cryst. Growth* **29** (1975) 137.
13. K. P. YOUNG and D. H. KIRKWOOD, *Metall. Trans. A*, **6A** (1975) 197.
14. Y. MIYATA, T. SUZUKI and J.-I. UNO, *Metall. Trans. A*, **16A** (1985) 1799.
15. U. FEURER, Int. Symp. Quality Control of Engineering Alloys and the Role of Metals Science, Delft, 1977, Netherland. Edited by N. Nieswaag and J.-W. Schwut. (Delft 1977, Netherland) p. 131.
16. T. Z. KATTAMIS and M. C. FLEMING, *TMS, AIME* **233** (1965) 992.
17. T. Z. KATTAMIS, J. C. COUGHLIN and M. C. FLEMING, *ibid.* **239** (1967) 1504.
18. J. R. CARRUTHERS, *J. Cryst. Growth* **32** (1976) 13.
19. W. R. WILCOX, *ibid.* **65** (1983) 133.
20. R. J. SCHAEFER and S. R. CORIEL, *Metall. Trans. A*, **15A** (1984) 2109.
21. S. R. CORIELL, M. R. CORDES, W. J. BOETTINGER and R. F. SEKERKA, *J. Cryst. Growth* **49** (1980) 13.
22. W. J. BOETTINGER, F. S. BIANCANIELLO and S. R. CORIEL, *Metall. Trans. A*, **12A** (1981) 321.
23. M. H. BURDEN, D. J. HEBDITCH and J. D. HUNT, *J. Cryst. Growth* **20** (1974) 121.
24. M. C. FLEMINGS, "Solidification Processing" (McGraw Hill, New York, 1974).
25. W. KURZ and D. J. FISHER, *Acta. Metall.* **29** (1981) 11.
26. K. SOMBOONSUK, J. T. MASON and R. TRIVEDI, *Metall. Trans. A*, **15A** (1984) 967.
27. J. S. LANGER and H. MULLER-KRUMBHAAR, *Acta. Metall.* **26** (1978) 1681.
28. J. D. VERHOEVEN, *TMS, AIME* **242** (1968) 1937.
29. J. D. HUNT, in Proceedings of Conference on Solidification. Sheffield, England, 18–21 July, 1977. (The Metals Society, Book 192, London 1979) p. 3.
30. E. A. FEEST, *J. Inst. Metals* **101** (1973) 279.

Received 7 January 1987
and accepted 13 March 1987